Nonequilibrium Phase Precursors during a Photoexcited Insulator-to-Metal Transition in V_{2}O_{3}

Andrej Singer, Juan Gabriel Ramirez, Ilya Valmianski, Devin Cela, Nelson Hua, Roopali Kukreja, James Wingert, Olesya Kovalchuk, James M. Glownia, Marcin Sikorski, Matthieu Chollet, Martin Holt, Ivan K. Schuller, and Oleg G. Shpyrko

Phys. Rev. Lett. **120**, 207601 — Published 14 May 2018

DOI: 10.1103/PhysRevLett.120.207601

Non-equilibrium phase precursors during a photoexcited insulator-to-metal transition in V_2O_3

Andrej Singer[1,*], Juan Gabriel Ramirez[1,2], Ilya Valmianski[1], Devin Cela[1], Nelson Hua[1], Roopali Kukreja[1], James Wingert[1], Olesya Kovalchuk[1], James M. Glownia[3], Marcin Sikiroski[3], Matthieu Chollet[3], Martin Holt[4], Ivan K. Schuller[1], and Oleg G. Shpyrko[1]

[1]*Department of Physics and Center for Advanced Nanoscience, University of California San Diego, La Jolla, California 92093, USA*

[2] *Department of Physics, Universidad de los Andes, Bogotá 111711, Colombia*

[3]*LCLS, SLAC National Accelerator Laboratory, Menlo Park, California 94025, USA*

[4]*Center for Nanoscale Materials, Argonne National Laboratory, Argonne, IL 60439, USA*

[*]*Present address: Department of Materials Science and Engineering, Cornell University, Ithaca, NY, 14850, USA*

Abstract

Here, we photoinduce and directly observe with x-ray scattering an ultrafast enhancement of the structural long-range order in the archetypal Mott system V_2O_3. Despite the ultrafast increase in crystal symmetry, the change of unit cell volume occurs an order of magnitude slower and coincides with the insulator-to-metal transition. The decoupling between the two structural responses in the time domain highlights the existence of a transient photoinduced precursor phase, which is distinct from the two structural phases present in equilibrium. X-ray nanoscopy reveals that acoustic phonons trapped in nanoscale blocks govern the dynamics of the ultrafast transition into the precursor phase, while nucleation and growth of metallic domains dictate the duration of the slower transition into the metallic phase. The enhancement of the long-range order before completion of the electronic transition demonstrates the critical role the non-equilibrium structural phases play during electronic phase transitions in correlated electrons systems.

Main Text

The discovery of novel phases of matter is at the core of modern physics. In quantum materials, subtle variations in atomic-scale interactions can dramatically alter the

macroscopic properties and drive phase transitions [1,2]; thus, recent research focused on using ultrafast photoexcitation in accessing out-of-equilibrium 'hidden' phases of matter in these systems [3–5]. Furthermore, ultrafast photoexcitation is unique in separating the roles of electronic [6] and average lattice response [5,7,8] in phase transitions, allowing a systematic investigation of the energy landscape. Despite their importance [9–13], the mesoscale processes underpinning phase transitions often remain elusive because of the vast differences in timescales between atomic and electronic changes and thermodynamic transformations. Here we combine ultrafast X-ray scattering in studying the dynamics and X-ray nanoscopy in studying the mesoscale heterogeneity during the photoexcited insulator-to-metal transition in V_2O_3.

Vanadium sesquioxide (V_2O_3) undergoes an insulator-to-metal transition upon heating at 160 K: the electric conductivity grows by five orders of magnitude (see Fig. S1 in [14]) via percolation of the high-temperature (HT) paramagnetic, metallic domains within the low-temperature (LT) antiferromagnetic, orbitally ordered, insulating domains [13,15–18]. The insulator-to-metal transition can be induced by temperature [19], pressure [19,20], electric field [21], and light [22–24]. The electronic phase transition is accompanied by a structural phase transition, where the crystal symmetry increases from monoclinic to rhombohedral, and the volume shrinks via reduction of the average hexagon edge from 2.91 Å to 2.87 Å (see Fig. 1**a**) [19,25,26]. While the symmetry and volume are coupled in equilibrium, here we show that ultrafast photoexcitation decouples these structural degrees of freedom, and the photoinduced phase transformation occurs via a non-equilibrium transient pathway (see Fig. 1**b**).

We study a 100 nm thin V_2O_3 film grown along the $(024)_{Rh}$ crystallographic direction. The steep slope of the resistivity versus temperature across the transition (factor of 100 over 5 K) and the total resistivity change of almost six orders of magnitude confirm the high quality of the films: poor crystallinity and disorder are detrimental to the insulator-to-metal transition [17]. The difference in the hexagon edge lengths results in two well distinct X-ray Bragg peaks along the film normal, $q_\perp$: $(024)_{Rh}$ and $(022)_{Mon}$ (see inset in Fig. 1**c**). The LT diffraction peak is broader than the HT peak in the direction parallel to

the film, $q_{\parallel}$ (see inset in Fig. 1**c**). The excess broadening results from a reduction of the long-range order (coherence length) due to the breaking of the crystal symmetry at low temperatures: three monoclinic structures are possible, each distorted along a different hexagon edge [19,25]. When heated quasi-statically through the phase transition temperature, the height of the HT peak grows, while the height of the LT peak decreases monotonically. The LT diffraction peak width is proportional to the LT peak height, while the width of the HT peak is static (see Fig. S2 in [14]).

We use short, optical laser pulses (E=1.55 eV, 40 fs duration, 500 μm spot size) to induce an insulator-to-metal phase transition in V_2O_3. We probe the structural response to photoexcitation with short x-ray pulses (E=9 keV, 10 fs duration, 200 μm spot size) in stroboscopic mode at the Linac Coherent Light Source [27,28]. After photoexcitation, the height of the HT peak grows as expected (see Fig. 1**c**), as the optical laser pulse heats the film. Because the HT peak grows, one may expect a drop in the LT peak height. Unexpectedly, the height of the LT peak grows for 2.5 ps before it declines for larger time delays (see Fig. 1**d**). From the 4D data set (3D reciprocal space and time, see Fig. S3 in [14]), we find that the LT peak height grows by narrowing the LT peak. Since the peak broadening in the ground state originates from the decrease in long range order, we conclude that photoexcitation induces higher symmetry in the LT phase after 2.5 ps. At these short timescales however, the photoexcited LT phase retains its unit cell volume, as revealed by the unmodified Bragg peak position (see Fig. 1**b**).

The photoinduced structural phase transition displays two processes with vastly different characteristic time scales. First, the structural coherence length in the photoexcited LT phase, $\xi(\tau)$, grows rapidly within 2.5 ps (see Fig 2**a**, left axis) and remains high for more than 100 ps. Second, the HT phase fraction, $P_{HT}(\tau)$, grows gradually within 100 ps after photoexcitation: the unit cell volume of the photoexcited LT regions shrinks discontinuously and the HT phase emerges, evidenced by decrease of the LT and increase of the HT integral peak intensity (see right axis in Fig. 2**a**, and Fig. S4 in [14]). Furthermore, the coherence length and the phase fraction depend differently on the pump fluence. The coherence length ξ(2.5ps) increases linearly with the pump fluence before it

saturates at ~5 mJ/cm^2 (see Fig. 2**b**). The dynamic saturation value at 1.3 above the ground state agrees with the maximum coherence length of the LT phase measured in equilibrium (see Fig. S2). In contrast, the final HT phase fraction P_{HT}(100 ps) displays a fluence threshold: the growth rate increases significantly for fluences larger than 1 mJ/cm^2 (see Fig. 2**c**). In photoinduced phase transitions, the fluence threshold results from the energy barrier due to the latent heat [4,6,22], and the value of 1 mJ/cm^2 measured here is in agreement with literature [22]. At fluences higher than 5 mJ/cm^2 the phase fraction P_{HT}(100 ps) saturates at its maximum value of one, when the entire volume is in the HT phase. While the presence of the fluence threshold and the duration of the HT phase growth are both consistent with the photoinduced electronic transition [22], the origin of the 2.5 ps time scale remains elusive. Similar timescale has been observed in time resolved x-ray experiments in bulk V_2O_3 crystals [24]. To understand the mechanism underpinning this ultrafast coherence length growth, we use X-ray nanoscopy.

We map the static nanoscale spatial distribution of the two structural phases (see Fig. 3**a**) and their coherence length (see Fig. S5 in [14]) by scanning a 20 nm X-ray beam across the sample [29]. The typical size of an LT domain (connected blue region in Fig. 3**a**) is 100 nm, consistent with near-field imaging of insulating and metallic pockets [13]. Surprisingly, the broadening of the LT diffraction peak is present in the diffraction collected during a single exposure by the 20nm nanobeam (see Fig. 3**b**). Thus, the monoclinic distortion reduces the long-range order on a length scale much smaller than the size of a LT domain. X-ray diffraction at higher angles (see Fig. S6 [14]) reveals splitting of the LT phase into a mosaic of two distinct types of crystallites angularly misaligned to each other by 1° about the film normal. The two categories correspond to monoclinic distortions either along the A or B directions (see Figs. 3**c** and Fig. S7 [14]). Statistical analysis of 20,000 diffraction patterns collected while scanning the nanobeam across the film [14] (see Fig. S8 in [14]) yields an average crystallite size of ξ=8 nm (see Fig. 3**c**). The spatially resolved peak broadening (see Fig. S5b in [14]) is independent of the LT peak intensity, suggesting a random distribution of the crystallites throughout the film. The diffraction peak corresponding to the monoclinic distortion along the third

direction appears at a different momentum transfer [25] and is only noticeable at the lowest temperatures.

The combination of time-resolved diffraction and x-ray nanoscopy implies that the photoexcited structural phase transition proceeds as follows (see Fig. 3**d**). Photoexcitation enhances the coherence length through a collective alignment of the crystallites within 2.5 ps. This ultrafast time scale (see Fig. 1**d**) is in agreement with the half period $\frac{\tau_P}{2} = \frac{L}{v} \approx 3.2\ ps$ of the coherent phonon at the Brillouin zone boundary [30], where L=8 nm is the size of the crystallite and $v = 2.5\ \mathrm{nm/ps}$ is the sound velocity in monoclinic V_2O_3 (Ref. [23]). The 8 nm large crystallites act as internal traps for acoustic phonons, which drive the symmetry enhancement by shear motion [3]. The degree of alignment grows linearly with pump fluence (see Fig. 2**b**), characteristic of a continuous phase transition as described by Landau theory extended to ultrafast transitions [31]. The photoinduced phase transition completes with a unit cell volume contraction within 100 ps, while the crystallites remain aligned with an enhanced coherence length. This longer process displays a fluence threshold: the hallmark of a first-order phase transition due to the latent heat [6,22]. The volume contraction is governed by the nucleation and ballistic growth through 100 nm large LT domains moving at the sound velocity [22] (see Fig. 3**a**).

Laser pulse energies well below the fluence threshold align the crystallites in the LT phase, yet avoid the transition into the HT phase (see Fig. S9 [14]). At these low fluences the enhanced long-range order prevails for more than 100 ps measured in our experiment. This duration represents the lower time scale for the spontaneous symmetry breaking into structurally equivalent monoclinic lattices, whose presence possibly stabilizes the transient higher symmetry phase. Above the fluence threshold, the coherence length enhancement and the HT phase fraction growth both saturate at 5 mJ/cm^2, indicating that the transient non-equilibrium state is a precursor to the metallic state.

In Mott insulators, the electronic correlations restrict the extent of the electronic wave function to a few nanometers [20,32]. The size of the monoclinic crystallites ξ we

determine from X-ray nanoscopy is in agreement with the electronic correlation length ξ_{el} found in bulk V_2O_3, Ref. [20]. The agreement between the length scales indicates an interdependence between the electronic localization and structural heterogeneity; we directly observe the latter as twinning of the LT phase into different monoclinic nanocrystallites in equilibrium. By assuming that the electronic correlation length and the crystallite size remain coupled after photoexcitation $\xi_{el}(\tau)=\xi(\tau)$, we estimate the behavior of the dynamic Mott gap via $\Delta(\tau)\sim 1/\xi(\tau)^2$ (Refs. [1,20]). The photoexcitation induces an ultrafast alignment of the crystallites, which effectively increases the coherence length and induces a narrowing of the band gap (see Fig. 3**D**). The correlation length increases by a factor of 1.3 at a pump fluence of 5 mJ/cm^2, thus the gap reduces from 0.5 eV in the ground state [33] below 0.3 eV in the photoexcited state. The maximum dynamic correlation length in the monoclinic phase is smaller than the correlation length in the rhombohedral phase; thus the gap is not closed entirely, consistent with the existence of a dynamic pseudogap observed in other Mott systems [34].

The photoexcited phase is structurally similar to the paramagnetic insulating phase, which in equilibrium occurs with chromium doping or equivalently with negative pressure [19,25,26]. In the monoclinic LT structure the vanadium magnetic moments ferromagnetically couple in monoclinic $(010)_{Mon}$ layers with a reversal of the adjacent layers; the moments tilt by 71 degrees from trigonal axis [15]. While recent theoretical calculations showed a decoupling between the antiferromagnetic ordering and monoclinic distortion, both phenomena reinforce each other [35]. The observation of the ultrafast quench of the monoclinic distortion indicates an ultrafast quench of the antiferromagnetic order. Furthermore, we expect the negative thermal expansion in V_2O_3 within the hexagon plane to results in a transient negative pressure after photoexcitation: in equilibrium, the negative pressure reduces the antiferromagnetic order and the monoclinic distortion [26]. The photoinduced insulator-to-metal transition in V_2O_3 lasts for tens of picoseconds [22], consistent with the duration of the structural unit cell volume change reported here. The long-range order enhancement through cooperative nanoscale alignment occurs before the electronic transition completes. Because long-

range order is essential for electronic transport [17], we anticipate that the presence of the photoinduced structural order impacts the dynamics of the electronic transition.

In summary, we used ultrafast x-ray scattering and x-ray nanoscopy in studying the photoinduced insulator-to-metal transition in V_2O_3. Using ultrafast x-ray scattering, we directly observe a novel photoinduced structural phase as a transient precursor to the metallic phase: photoexcitation rapidly enhances the long-range order in the insulating phase before the photoexcited material transitions to the metallic phase. We observed no indication of the transient phase during the quasi-static phase transformation. Using high-resolution x-ray nanoscopy at near-5 nm resolution, we are able to correlate the evolution of the structural heterogeneity to the extent of the electronic wave function and the Mott gap. By combining the results from ultrafast x-ray scattering and x-ray nanoscopy we elucidate how the nanoscale heterogeneity influences the time scales of the photoexcited transition, suggesting a new path to controlling the energy landscape in strongly correlated electron systems.

Figures

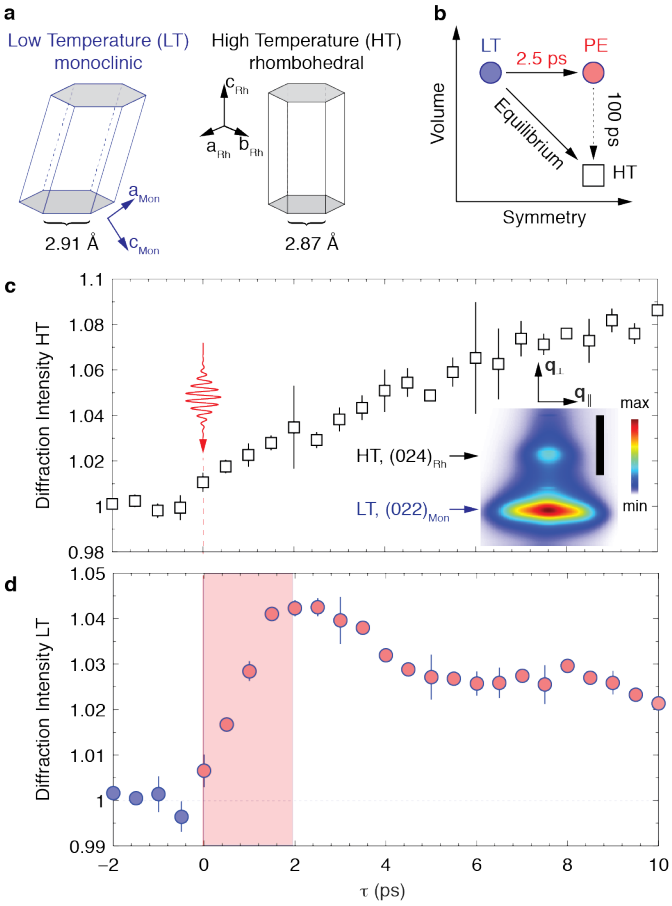

Figure 1: Temperature induced and photoinduced structural phase transition. **a,** The monoclinic insulating and rhombohedral metallic structures. The hexagon corners represent vanadium atoms. Oxygen and other vanadium atoms within the shown structures are omitted for better visibility. **b,** Schematic phase diagram of two equilibrium low-temperature (LT) and high-temperature (HT) phases and the photoexcited (PE) phase. In equilibrium, the transition occurs directly from LT to HT, while photoinduced transition occurs via a transient, non-equilibrium phase. **c, d,** The peak intensity of the HT, $(024)_{Rh}$ diffraction peak (**c**) and of the LT, $(022)_{Mon}$ diffraction peak (**d**) as a function of the time delay after photoexcitation (pump fluence 1 mJ/cm^2) at a base temperature of 157 K. Inset in **c**: A slice through the 3D diffracted intensity around both peaks (linear scale). $q_\perp$ is parallel to $(024)_{Rh}$ and $q_{||}$ to $(-210)_{Rh}$. Scale bar shows 0.04 Å^{-1}. The uncertainties in **c, d** result from the difference between two independent measurements.

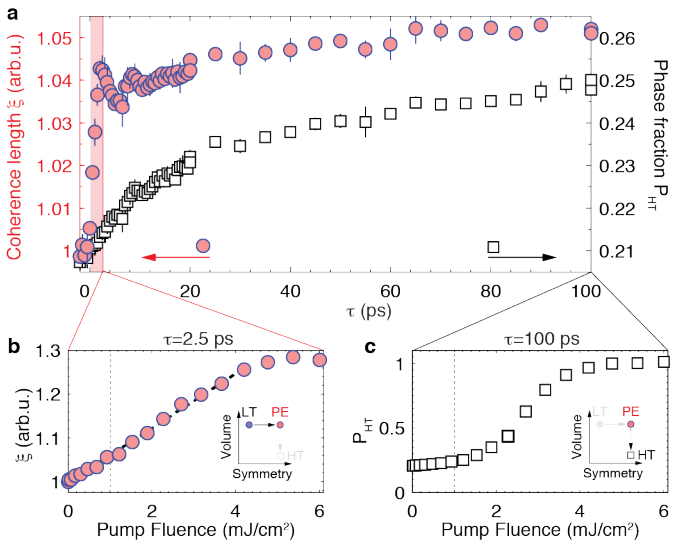

Figure 2: Fluence dependence of the photoinduced structural phase transition. a, Time dependence of the coherence length ξ (filled red circles, left axis) calculated as the reciprocal peak width with a fluence of 1 mJ/cm^2 and the HT phase fraction $P_{HT}=V_{HT}/(V_{HT+}V_{LT})$ (open black squares, right axis), where V_{HT} and V_{LT} are the HT and LT peak integral intensities. **b,** The coherence length 2.5 ps after photoexcitation as a function of the laser pump fluence. **c,** The HT phase fraction 100 ps after photoexcitation normalized to the value at highest fluences, where the entire film is metallic. Insets show the schematic path from LT to photoexcited (PE) phase **b** and PE to HT phase **c**.

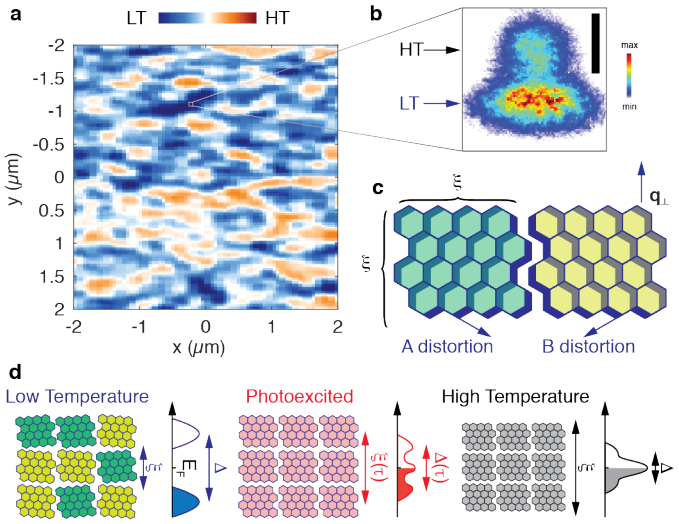

Figure 3: Nanoscale description of the dynamic phase transition. a, Measured spatial distribution of the LT phase in equilibrium determined from the integral intensity of the LT diffraction peak, $I_{LT}(x,y)$. The spatial distributions of the HT phase ($I_{HT}(x,y)$, not shown) is anti-correlated to the LT phase distribution with a Pearson correlation coefficient of $\frac{\int I_{LT}(x,y)\cdot I_{HT}(x,y)dxdy}{\sqrt{(\int I_{LT}(x,y)^2 dxdy)(\int I_{HT}(x,y)^2 dxdy)}} = -0.58 \pm 0.01$ (complete segregation yields a value of -1 and complete intermixing a value of 0). **b** A typical diffraction pattern measured during a single exposure to the nanobeam with a spot size of 20 nm (linear scale). Scale bar shows 0.04 $Å^{-1}$. **c** Schematic of two neighboring monoclinic domains with distortions along different hexagon edges A and B. The monoclinic distortion and the physical touching of the mosaic blocks results in an angular misalignment. The size of the monoclinic domains is ξ=8 nm. **d** Schematic evolution of the structure and the proposed dynamics of the electronic properties during the photoinduced phase transition. (Left panel) In the low temperature ground state the crystallites are misaligned, and the electronic system is gapped. (Middle panel) Photoexcitation raises the coherence length through alignment of the crystallites and partially closes the Mott gap. (Right panel) The volume changes discontinuously, the Mott gap closes and the equilibrium metallic state emerges.

Acknowledgements
We thank Lu Sham, Marcelo Rozenberg, and Richard Averitt for discussions, and thank Eric Fullerton for pointing out the significance of the negative thermal expansion during the phase transition. The work at UCSD was supported by the AFOSR grant #FA9550-16-1-0026 and a UC collaborative grant MRPI MR-15-328-528. The work at UCSD was supported by U.S. Department of Energy, Office of Science, Office of Basic Energy Sciences, under Contracts No. DE - SC0001805 (x-ray scattering A.S., D.C., N.H., R.K., O.K., J.W., and O.G.S.) and No. DE FG02 87ER-45332 (thin film synthesis and characterization J.G.R., I.V., and I.K.S.). J.G.R. acknowledges support from FAPA program through Facultad de Ciencias and Vicerrectoria de Investigaciones of Universidad de los Andes, Bogotá Colombia and Colciencias #120471250659 and #120424054303. Use of the Linac Coherent Light Source (LCLS), SLAC National Accelerator Laboratory, is supported by the U.S. Department of Energy, Office of Science, Office of Basic Energy Sciences under Contract No. DE-AC02-76SF00515. Use of the Advanced Photon Source and the Center for Nanoscale Materials, both Office of Science User Facilities, was supported by the US Department of Energy, Office of Science, Office of Basic Energy Sciences, under Contract No. DE-AC02-06CH11357.

Author contributions
A.S and J.G.R. conceived of the idea. A.S., J.G.R., I.K.S., and O.G.S planned the experiment. J.G.R. and I.V. prepared the samples, characterized them and performed resistance measurements for the in-situ temperature calibration. A.S, J.G.R, I.V., D.C, N.H., R.K., O.K., J.M.G., M.S., M.Ch., and O.G.S. conducted the time resolved experiment. A.S., N.H., J.W., and M.H. conducted the nanodiffraction experiment. A.S. analyzed the data. All authors discussed the interpretation of the data. A.S., J.G.R., I.V., and D.C. wrote the initial version of the paper. The paper underwent multiple revisions by all authors.

References

[1] M. Imada, A. Fujimori, and Y. Tokura, Rev. Mod. Phys. **70**, 1039 (1998).

[2] E. Dagotto, Science **309**, 257 (2005).

[3] P. Baum, D.-S. Yang, and A. H. Zewail, Science **318**, 788 (2007).

[4] V. R. Morrison, R. P. Chatelain, K. L. Tiwari, A. Hendaoui, A. Bruhács, M. Chaker, and B. J. Siwick, Science **346**, 445 (2014).

[5] J. Zhang, X. Tan, M. Liu, S. W. Teitelbaum, K. W. Post, F. Jin, K. A. Nelson, D. N. Basov, W. Wu, and R. D. Averitt, Nat. Mater. **15**, 956 (2016).

[6] A. Pashkin, C. Kübler, H. Ehrke, R. Lopez, A. Halabica, R. F. Haglund, R. Huber, and A. Leitenstorfer, Phys. Rev. B **83**, 195120 (2011).

[7] M. Porer, U. Leierseder, J.-M. Ménard, H. Dachraoui, L. Mouchliadis, I. E. Perakis, U. Heinzmann, J. Demsar, K. Rossnagel, and R. Huber, Nat. Mater. **13**, 857 (2014).

[8] A. Singer, S. K. K. Patel, R. Kukreja, V. Uhlíř, J. Wingert, S. Festersen, D. Zhu, J. M. Glownia, H. T. Lemke, S. Nelson, M. Kozina, K. Rossnagel, M. Bauer, B. M. Murphy, O. M. Magnussen, E. E. Fullerton, and O. G. Shpyrko, Phys. Rev. Lett. **117**, 56401 (2016).

[9] M. Fratini, N. Poccia, A. Ricci, G. Campi, M. Burghammer, G. Aeppli, and A. Bianconi, Nature **466**, 841 (2010).

[10] Y. Kohsaka, T. Hanaguri, M. Azuma, M. Takano, J. C. Davis, and H. Takagi, Nat. Phys. **8**, 534 (2012).

[11] I. Zeljkovic, Z. Xu, J. Wen, G. Gu, R. S. Markiewicz, and J. E. Hoffman, Science **337**, 320 (2012).

[12] G. Campi, A. Bianconi, N. Poccia, G. Bianconi, L. Barba, G. Arrighetti, D. Innocenti, J. Karpinski, N. D. Zhigadlo, S. M. Kazakov, M. Burghammer, M. v. Zimmermann, M. Sprung, and A. Ricci, Nature **525**, 359 (2015).

[13] A. S. McLeod, E. van Heumen, J. G. Ramirez, S. Wang, T. Saerbeck, S. Guenon, M. Goldflam, L. Anderegg, P. Kelly, A. Mueller, M. K. Liu, I. K. Schuller, and D. N. Basov, Nat. Phys. **13**, 80 (2016).

[14] See supplementary material at [URL will be inserted by publisher] for experimental description, details on recording and analyzing the 4D dataset, diffraction at higher q values, statistical analysis of the nanodiffraction data, and supplementary figures, which includes Refs. [36-39].

[15] M. Moon, Phys. Rev. Lett. **8**, 527 (1970).

[16] L. Paolasini, C. Vettier, F. de Bergevin, F. Yakhou, D. Mannix, A. Stunault, W. Neubeck, M. Altarelli, M. Fabrizio, P. A. Metcalf, and J. M. Honig, Phys. Rev. Lett. **82**, 4719 (1999).

[17] J. G. Ramirez, T. Saerbeck, S. Wang, J. Trastoy, M. Malnou, J. Lesueur, J.-P. Crocombette, J. E. Villegas, and I. K. Schuller, Phys. Rev. B **91**, 205123 (2015).

[18] J. de la Venta, S. Wang, T. Saerbeck, J. G. Ramírez, I. Valmianski, and I. K. Schuller, Appl. Phys. Lett. **104**, 62410 (2014).

[19] D. B. McWhan and J. P. Remeika, Phys. Rev. B **2**, 3734 (1970).

[20] P. Limelette, A. Georges, D. Jerome, P. Wzietek, P. Metcalf, and J. M. Honig, Science **302**, 89 (2003).

[21] G. Mazza, A. Amaricci, M. Capone, and M. Fabrizio, Phys. Rev. Lett. **117**, 176401 (2016).

[22] E. Abreu, S. Wang, J. G. Ramírez, M. Liu, J. Zhang, K. Geng, I. K. Schuller, and R. D. Averitt, Phys. Rev. B **92**, 85130 (2015).
[23] E. Abreu, S. N. Gilbert Corder, S. J. Yun, S. Wang, J. G. Ramírez, K. West, J. Zhang, S. Kittiwatanakul, I. K. Schuller, J. Lu, S. A. Wolf, H.-T. Kim, M. Liu, and R. D. Averitt, Phys. Rev. B **96**, 94309 (2017).
[24] G. Lantz, B. Mansart, D. Grieger, D. Boschetto, N. Nilforoushan, E. Papalazarou, N. Moisan, L. Perfetti, V. L. R. Jacques, D. Le Bolloc'h, C. Laulhé, S. Ravy, J. P. Rueff, T. E. Glover, M. P. Hertlein, Z. Hussain, S. Song, M. Chollet, M. Fabrizio, and M. Marsi, Nat. Commun. **8**, 1 (2017).
[25] P. D. Dernier and M. Marezio, Phys. Rev. B **2**, 3771 (1970).
[26] D. B. McWhan, A. Menth, J. P. Remeika, W. F. Brinkman, and T. M. Rice, Phys. Rev. B **7**, 1920 (1973).
[27] P. Emma, R. Akre, J. Arthur, R. Bionta, C. Bostedt, J. Bozek, A. Brachmann, P. Bucksbaum, R. Coffee, F.-J. Decker, Y. Ding, D. Dowell, S. Edstrom, A. Fisher, J. Frisch, S. Gilevich, J. Hastings, G. Hays, HeringPh., Z. Huang, R. Iverson, H. Loos, M. Messerschmidt, A. Miahnahri, S. Moeller, H.-D. Nuhn, G. Pile, D. Ratner, J. Rzepiela, D. Schultz, T. Smith, P. Stefan, H. Tompkins, J. Turner, J. Welch, W. White, J. Wu, G. Yocky, and J. Galayda, Nat Phot. **4**, 641 (2010).
[28] D. Zhu, Y. Feng, S. Stoupin, S. A. Terentyev, H. T. Lemke, D. M. Fritz, M. Chollet, J. M. Glownia, R. Alonso-Mori, M. Sikorski, S. Song, T. B. van Driel, G. J. Williams, M. Messerschmidt, S. Boutet, V. D. Blank, Y. V Shvyd'ko, and A. Robert, Rev. Sci. Instrum. **85**, 63106 (2014).
[29] R. P. Winarski, M. V. Holt, V. Rose, P. Fuesz, D. Carbaugh, C. Benson, D. Shu, D. Kline, G. B. Stephenson, I. McNulty, and J. Maser, J. Synchrotron Radiat. **19**, 1056 (2012).
[30] H. Park, X. Wang, S. Nie, R. Clinite, and J. Cao, Phys. Rev. B **72**, 100301 (2005).
[31] P. Beaud, A. Caviezel, S. O. Mariager, L. Rettig, G. Ingold, C. Dornes, S.-W. Huang, J. A. Johnson, M. Radovic, T. Huber, T. Kubacka, A. Ferrer, H. T. Lemke, M. Chollet, D. Zhu, J. M. Glownia, M. Sikorski, A. Robert, H. Wadati, M. Nakamura, M. Kawasaki, Y. Tokura, S. L. Johnson, and U. Staub, Nat. Mater. **13**, 923 (2014).
[32] H. Yamakawa, T. Miyamoto, T. Morimoto, T. Terashige, H. Yada, N. Kida, M. Suda, H. M. Yamamoto, R. Kato, K. Miyagawa, K. Kanoda, and H. Okamoto, Nat. Mater. **16**, 1100 (2017).
[33] M. M. Qazilbash, A. A. Schafgans, K. S. Burch, S. J. Yun, B. G. Chae, B. J. Kim, H. T. Kim, and D. N. Basov, Phys. Rev. B **77**, 115121 (2008).
[34] C. Sohrt, A. Stange, M. Bauer, and K. Rossnagel, Faraday Discuss. **171**, 243 (2014).
[35] D. Grieger and M. Fabrizio, Phys. Rev. B **92**, 75121 (2015).
[36] A. Sharoni, J. G. Ramírez, and I. K. Schuller, Phys. Rev. Lett. **101**, 26404 (2008).
[37] G. J. Williams, M. A. Pfeifer, I. A. Vartanyants, and I. K. Robinson, Phys. Rev. Lett. **90**, 175501 (2003).
[38] G. K. Williamson and W. H. Hall, Acta Metall. **1**, 22 (1953).
[39] M. A. Moram and M. E. Vickers, Reports Prog. Phys. **72**, 36502 (2009).